Asian Journal of Chemistry; Vol. 32, No. 9 (2020), 2222-2228

ASIAN JOURNAL OF CHEMISTRY

https://doi.org/10.14233/ajchem.2020.22744

Spectroscopic Properties, Magnetic Behaviours and Hirshfeld Surface Analysis of Ag[Cr(1,3-pdta)]·3H$_2$O

SUNGHWAN JEON[1], SHINNOSUKE TANAKA[2], TAKASHIRO AKITSU[2], KEON SANG RYO[1] and JONG-HA CHOI[1,*]

[1]Department of Chemistry, Andong National University, Andong 36729, Republic of Korea
[2]Department of Chemistry, Tokyo University of Science, Tokyo 162-8601, Japan

*Corresponding author: E-mail: jhchoi@anu.ac.kr

Received: 27 March 2020; *Accepted*: 27 May 2020; *Published online*: 20 August 2020; AJC-20016

The presence of various functional groups present in Ag[Cr(1,3-pdta)]·3H$_2$O (1,3-pdta = 1,3-propanediaminetetraacetate) was confirmed by FT-IR spectral results. The electronic spectral properties and magnetic behaviours were also described. The results of our calculations yielded the crystal field splitting and Racah parameters of Dq = 1969 cm^{-1}, B = 594 cm^{-1} and C = 3250 cm^{-1}. Hirshfeld surface analysis by three-dimensional (3D) molecular surface contours and two-dimensional (2D) fingerprint plots were performed to visualize, explore and quantify the intermolecular interactions in the crystal lattice. Hirshfeld surface contours and 2D fingerprint maps revealed that the crystal packing is dominated by H···O/O···H and H···H contacts. The strong hydrogen-bonding interactions are linked with O–H···O consisting the highest fraction of 63.4% followed by these of the H···H type contributing 25.5%. Other very weak contacts of Ag···O/O···Ag, C···H/H···C, O···O, Ag···H/H···Ag and O···C/C···O are present in the title compound.

Keywords: Chromium(III) complex, Electronic absorption spectroscopy, Magnetic properties, Hirshfeld surface analysis.

INTRODUCTION

Chromium exists in water in various oxidation states from 0 to VI. In natural water, the most common form is Cr(III), principally presents as an aqua-ion, and Cr(VI), mainly in the chromate ion, CrO_4^{2-} or dichromate ion, $Cr_2O_7^{2-}$. The toxicity of chromium compounds mainly depends on the oxidation state of the metal ion. The chromate and dichromate ions are highly cytotoxic substance and a potential carcinogen [1-3]. A number of treatment methods for the removal of toxic heavy metal ions in water including photocatalytic reduction Cr(VI) to Cr(III) have been described [4-6]. It may be possible that 1,3-propanediaminetetraacetate (1,3-pdta) is suitable reagent to target various toxic metal ions. Furthermore, compounds containing Cr(III) ion are promising materials for tunable solid-state lasers that emit in the spectral region between 700 and 1100 nm [7]. These chromium(III) compounds are also utilized as a storage material for highly efficient solar energy because those have a long lifetime in an excited state [8]. A detailed study of the spectroscopic and ligand field properties of these materials is required for this application. It has been recognized that the *d-d* transitions may be useful in determining metal-ligand bonding properties as well as molecular geometries [9-17]. In a recent communication, synthesis and crystal structural characterization of Ag[Cr(1,3-pdta)]·3H$_2$O is reported (Fig. 1) [18].

The complex crystallized in the orthorhombic space group $P2_12_12_1$ with Z = 4. It consists of one [Cr(1,3-pdta)]$^-$ anion, one silver cation and three water molecules. For convenience, a perspective drawing of [Cr(1,3-pdta)]$^-$ anion together with the atomic labeling is depicted in Fig. 2. It was found that 1,3-propanediaminetetraacetate octahedrally coordinate to the Cr metal center through four O and two N atoms. The average Cr–N and Cr–O bond lengths are 2.0727 (17) and 1.9608 (15) Å, respectively. The conformations of the chelate (R and G) rings for two glycinates were found to be an *envelope*. The six membered 1,3-propanediamine (T) ring takes a symmetric *skew-boat* form with λ conformation. The silver atom is surrounded octahedrally by three O atoms of 1,3-pdta groups and three water O atoms. However, the detailed physical properties of the complex have not been published yet.

In this article, the spectroscopic and magnetic studies of title compound using UV- visible, IR spectroscopy and temp-

This is an open access journal, and articles are distributed under the terms of the Attribution 4.0 International (CC BY 4.0) License. This license lets others distribute, remix, tweak, and build upon your work, even commercially, as long as they credit the author for the original creation. You must give appropriate credit, provide a link to the license, and indicate if changes were made.

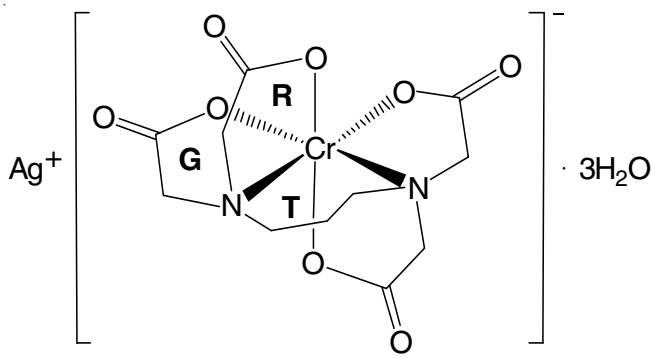

Fig. 1. Chemical structure of Ag[Cr(1,3-pdta)]·3H$_2$O

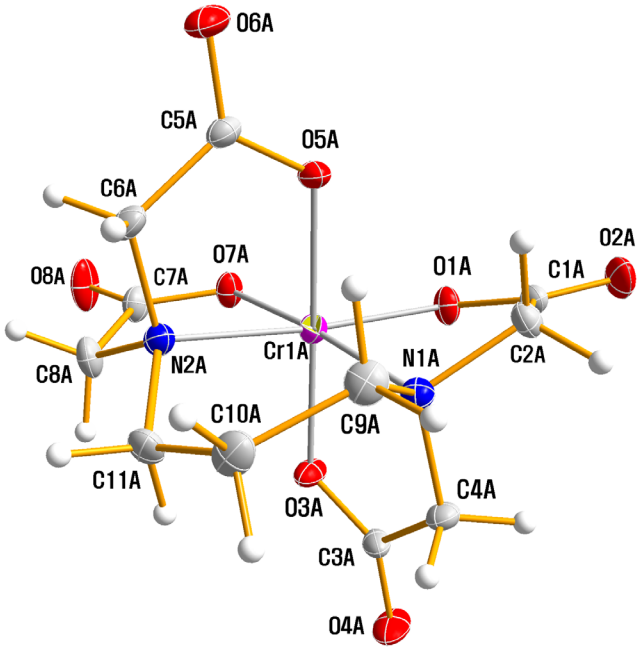

Fig. 2. Molecular structure of [Cr(1,3-pdta)]$^-$ anion in silver trihydrate salt

erature dependent magnetic susceptibility measurement are reported. The intermolecular interactions are also investigated using Hirshfeld surface analysis and 2D fingerprint plots.

EXPERIMENTAL

Synthesis: Chromium(III) nitrate trihydrate, $Cr(NO_3)_3 \cdot 3H_2O$ (99%) was purchased from Sigma-Aldrich and used without further purification. All other chemicals were reagent grade materials and used as received. Ag[Cr(1,3-pdta)]·3H$_2$O was synthesized as described earlier [18]. Before the measurements of various spectra were recorded, the complex was purified from aqueous solution by recrystallization. Elemental anal. calcd. (found) % of Ag[Cr($C_{11}H_{14}N_2O_8$)]·3H$_2$O: C, 25.93 (25.60); H, 3.12 (3.91); N, 5.38 (5.43). The visible spectral data for an aqueous solution, λ_{max} in nm (ε in M^{-1} cm^{-1}) are as follows: 201 (600), 223 (608), 245 (453), 385 (160), 508 (218), 700 (7). IR data (KBr, cm^{-1}): 3447 (*vs, br*) (ν OH), 3232 (*sh*), 2977 (*vs*) and 2941 (*s*) (ν CH), 1643 (*s, br*) (ν_{as} COO), 1473 (*s*) (δ CH_2), 1428 (*m*) (ν_s COO), 1363 (*vs*) and 1327 (*vs*), 1271 (*sh*), 1222 (*s*), 1144 (*s*) (ν CN), 1099 (*vs*), 1061 (*m*), 1029 (*s*), 988 (*s*), 941 (*vs*), 916 (*vs*), 897 (*m*) and 853 (*vs*), (ρ CH_2), 746 (*vs*), 690 (*m*), 632 (*w*), 579 (*m*), 529 (*s*), 486 (*s*), 433 (*s*) (ν Cr–N).

Physical measurements: The UV-visible absorption spectrum was recorded using an HP 8453 diode array spectrophotometer. The mid-infrared spectrum was obtained from a KBr pellet using a JASCO 460 plus series FT-IR spectrometer. The magnetic properties were investigated with a Quantum Design MPMS-XL superconducting quantum interference device SQUID magnetometer at an applied field of 0.5 T and a temperature range of 5-300 K. Powder samples were measured in a pharmaceutical cellulose capsule. Diamagnetic correction was applied with Pascal's method. Analyses for C, H and N were performed on a Perkin-Elmer 2400II CHNS/O analyzer at Tokyo University of Science, Tokyo, Japan

RESULTS AND DISCUSSION

IR spectroscopy: The IR spectrum of Ag[Cr(1,3-pdta)]·3H$_2$O (Fig. 3) was recorded at room temperature for the wavenumber region between 4000 and 400 cm^{-1}. The FT-IR spectrum contains a very strong absorption band at 3447 cm^{-1}, along with an additional shoulder band at 3232 cm^{-1} due to O-H stretching mode of three hydrate water molecules. The broadness of the IR bands is probably due to the existence of strong hydrogen bonds in the crystal. Strong bands in the 3000-2800 cm^{-1} region were attributed to the symmetric and anti-symmetric C-H stretching modes [4-11]. The asymmetric stretching carboxylate frequencies have been established as criteria for distinguishing between protonated carboxylate (1750-1700 cm^{-1}) and coordinated carboxylate (1650-1600 cm^{-1}). In general, two bands are expected due to the asymmetric vibrations of five-membered glycinato rings and six-membered β-alaninato rings. However, due to mixing with lattice water vibrations, all clear vibrations were not observed.

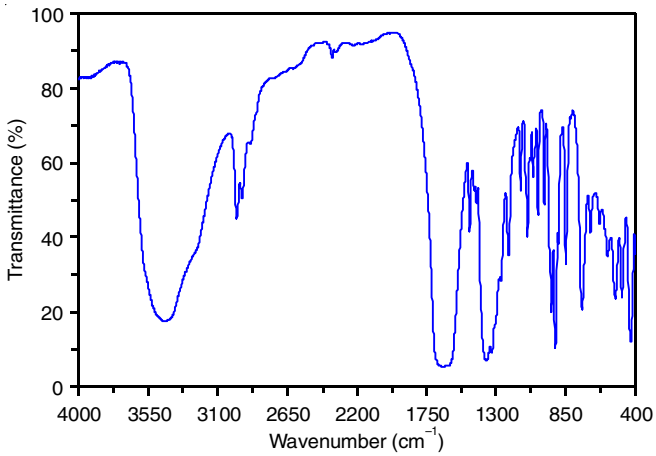

Fig. 3. FT-IR spectrum of Ag[Cr(1,3-pdta)]·3H$_2$O

The IR spectrum shows one strong broad band centered at 1643 cm^{-1} due to asymmetric stretching carboxylate, ν_{as}(COO). The lack of other absorptions in the 1750-1700 cm^{-1} range suggests that all the carboxylates are coordinated. The medium absorption band at 1473 cm^{-1} can be assigned to the CH_2 scissoring mode. The absorption at 1428 cm^{-1} is assigned to ν_s(COO). Various CH_2 wagging and twisting vibrations as well as some

skeletal modes occur in the region 1400-1000 cm^{-1}. The strong absorption at 1099 cm^{-1} may be attributed to the skeletal mode involving C-N stretching. The strong peak at 433 cm^{-1} can be assigned to the Cr-N stretching mode.

Electronic absorption spectroscopy: The three lowest terms of the Cr(III) free ion $3d^3$ configuration, *i.e.* ^4F, ^4P and ^2G (^4F is the ground state) are reduced in an octahedral environment as follows:

$$^4F \rightarrow {}^4A_{2g} + {}^4T_{2g} + {}^4T_{1g}$$

$$^4P \rightarrow {}^4T_{1g}$$

$$^2G \rightarrow {}^2E_g + {}^2T_{1g} + {}^2T_{2g} + {}^2A_{1g}$$

In case of chromium(III) complex with octahedral symmetry, several transitions due to spin-allowed and spin-forbidden are possible as shown in Fig. 4.

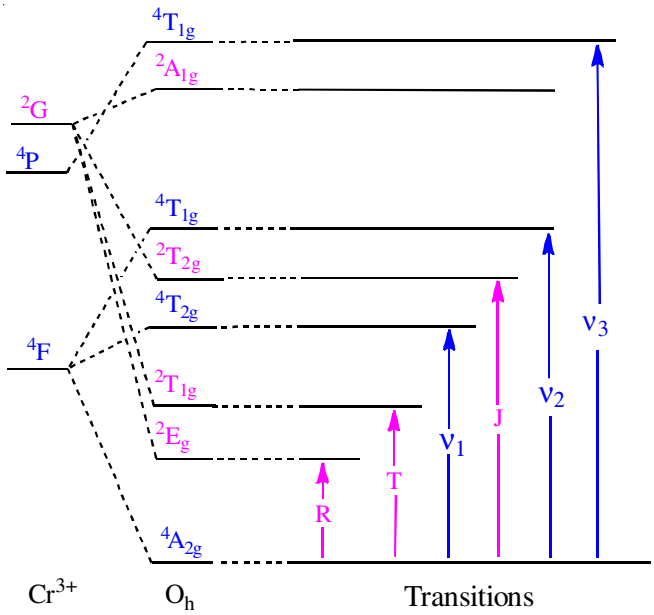

Fig. 4. State energy level diagram and electronic transitions of chromium(III) complex with octahedral symmetry

The UV-visible spectrum of $Ag[Cr(1,3\text{-pdta})]\cdot 3H_2O$ in aqueous solution is shown in Fig. 5. The third band corresponding to the $^4A_{2g} \rightarrow {}^4T_{1g}$ (^4P) transition in the complex anion $[Cr(1,3\text{-pdta})]^-$ are believed to be obscured by the intense bands of the charge transfer absorptions. In order to have some point of reference for the splitting of the electron bands, we have fitted the band profiles using four main Gaussian curves. A deconvolution procedure on the experimental band pattern yielded maxima at 18,795, 20,350, 25,200 and 26,250 cm^{-1} for $Ag[Cr(1,3\text{-pdta})]\cdot 3H_2O$.

In Fig. 5, two intense bands (blue line) located at 19,685 and 25,975 cm^{-1} correspond to $^4A_{2g} \rightarrow {}^4T_{2g}$ (ν_1) and $^4A_{2g} \rightarrow {}^4T_{1g}$ (^4F) (ν_2) transitions for $[Cr(1,3\text{-pdta})]^-$ ion. The electronic band positions for the $[Cr(1,3\text{-pdta})]^-$ moiety are good in agreement with those reported for $Na[Cr(1,3\text{-pdta})]\cdot 3H_2O$, $K[Cr(1,3\text{-pdta})]\cdot H_2O$ and $Ca[Cr(1,3\text{-pdta})]_2\cdot 4H_2O$ [19].

For octahedral d^3 system, the formula between three spin-allowed electronic transition energies and ligand field parameters is as follows [20]:

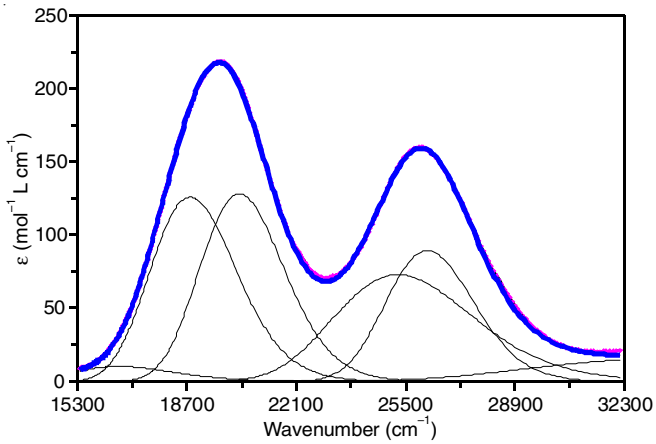

Fig. 5. Electronic absorption spectrum (blue line) and its resolved overlapping peaks (black line) of $Ag[Cr(1,3\text{-pdta})]\cdot 3H_2O$ in aqueous solution

$$^4A_{2g} \rightarrow {}^4T_{2g},\ \nu_1 = 10Dq \quad (1)$$

$$^4A_{2g} \rightarrow {}^4T_{1g}\ (^4F),\ \nu_2 = 7.5B + 10Dq - 1/2(225B^2 + 100Dq^2 - 180Dq \times B)^{1/2} \quad (2)$$

$$^4A_{2g} \rightarrow {}^4T_{1g}\ (^4P),\ \nu_3 = 7.5B + 15Dq + 1/2(225B^2 + 100Dq^2 - 180Dq \times B)^{1/2} \quad (3)$$

The first spin allowed transition directly gives the value of 10Dq. For $[Cr(1,3\text{-pdta})]^-$ moiety, the crystal field splitting parameter, Dq and Racah interelectronic repulsion parameter, *B* were obtained as 1969 cm^{-1} and 594 cm^{-1}, respectively. These parameters were calculated from the values of ν_1 and ν_2 by means of eqns. 4 and 5.

$$Dq = \frac{\nu_1}{10} \quad (4)$$

$$B = \frac{2\nu_1^2 + \nu_2^2 - 3\nu_1\nu_2}{15\nu_2 - 27\nu_1} \quad (5)$$

The change in B from the free ion value is expressed as the nephelauxetic ratio, β, which is given by eqn. 6.

$$\beta = \frac{B\ (complex)}{B_0\ (free\ \ ion)} \quad (6)$$

where B_0 is the Racah parameter for the free metal ion and B is the same parameter for metal ion in the complex [21]. The value of the Racah parameter, B for the title complex is about 65% of the value for a free chromium(III) ion in the gas phase. The β value indicates that there is an appreciable covalent character in the metal-ligand σ bond.

A very weak spin-forbidden $^4A_{2g} \rightarrow {}^2E_g$ (R) band was also observed at 14,285 cm^{-1}, but could not be resolved into separate components. The Racah parameter, C can be calculated from the position of $^4A_{2g} \rightarrow {}^2E_g$ absorption band and the eqn. 7 [22].

$$C = (B/3.05)[\{E(^2E_g)/B\} - 7.90 + 1.80(B/Dq)] \quad (7)$$

The value of C is evaluated to be 3250 cm^{-1}, which is significantly reduced from the free ion value of Cr(III), C_0 (free ion) = 4133 cm^{-1}. A comparsion of the two values reveals that C is decreased by 21% from C_0 (free ion) [11]. This decrease is also due to effect of bond covalency. The values of Dq, B and

C parameters obtained are comparable to those reported for $[Cr(chxn)_3]^{3+}$ (Dq = 2175 cm^{-1}, B = 703 cm^{-1} and C = 2953 cm^{-1}) [23]. The spin-orbit coupling can be calculated from the Cole and Garret empirical relation [24].

$$\lambda_{eff} = 11 \times 10^{-9} (B + 1080)^3 + 6.2 \quad (8)$$

Using B and eqn. 8 yields λ_{eff} = 58 cm^{-1}, which is in good agreement with the value expected for chromium(III) ion in crystals [24]. The deviation of λ_{eff} from λ_0 (87 cm^{-1} for free ion) is due to the bonding effects of urea ligands toward chromium(III) ion in the crystal [25].

Magnetic properties: The magnetic susceptibility of Ag[Cr(1,3-pdta)]·3H$_2$O was measured in the temperature range of 5-300 K at 10 kOe. The plot of χ_MT *vs.* T is shown in Fig. 6. The value of χ_MT at 300 K is 30.9 cm^3 K mol^{-1}. On decreasing the temperature, the χ_MT value slightly increases to a maximum of 34.3 cm^3 K mol^{-1} at 50 K and decreases again down to 30.1 cm^3 K mol^{-1} at 5 K. The effective magnetic moment values, λ_{eff}, were calculated from the eqn. 9:

$$\mu_{eff} = 2.83(\chi_M T)^{1/2} \quad (9)$$

where χ_M is the molar magnetic susceptibility (emu mol^{-1}) and T is the absolute temperature

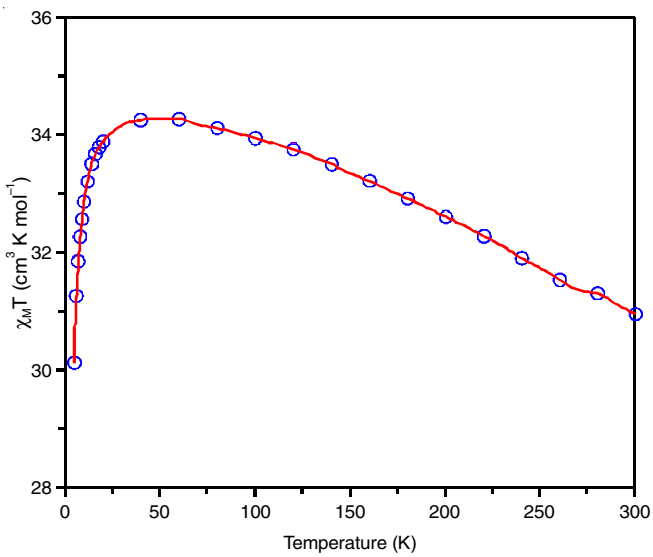

Fig. 6. Temperature-dependent magnetic susceptibility of Ag[Cr(1,3-pdta)]·3H$_2$O measured at 10 kOe

The observed effective magnetic moments are in the range 4.38 μ_B – 4.67 μ_B. The chromium(III) ion ($3d^3$) has three unpaired electrons in the 3*d* shell, but present compound has a larger magnetic moment than the spin-only value, 3.88 μ_B with *S* = 3/2 spin state of a mononuclear Cr(III) d^3 center [26].

Hirshfeld surface analysis: Hirshfeld surface analysis and two-dimensional (2D) fingerprint plot serve as invaluable tools for gaining additional insight into intermolecular interactions influential in the packing of molecules in crystals [27]. The Hirshfeld surface analysis and 2D fingerprint plot were performed using the Crystal Explorer program [28]. The molecular Hirshfeld surface and 2D fingerprint plots were used for quantitative mapping out these interactions [29-33]. The Hirshfeld surface can be mapped with different properties namely, d_{norm}, electrostatic potential, shape-index and curvedness. The d_{norm} surface shows identification of very close intermolecular interactions. On the contrary, the shape index is the most sensitive to very delicate changes in surface shape. The curvedness provides the shape of molecules. The flat areas of the surface stand for the low values of curvedness while the sharp ones indicate the high values of it. The molecular d_{norm} surface, shape index and curvedness are shown in Fig. 7.

The Hirshfeld surface plotted over d_{norm} utilize the function of normalized distances d_i and d_e, where d_i and d_e are the distances from a given point on the surface to the nearest atom inside and outside, respectively. In Fig. 7a, the white surface indicates contacts with distances equal to the sum of van der Waals radii, and the red and blue colours indicate distances shorter or longer than the van der Waals radii, respectively. Hirshfeld surface contours and 2-D fingerprint plots of major interactions are shown in Figs. 8-12, respectively. The d_{norm} surface shows the red, white and blue spots for main contacts due to O···H/ H···O interactions. The strongest hydrogen-bonding interactions are linked with O–H···O consisting the highest fraction of 63.4% followed by these of the H···H type contributing 25.5%. Apart from these above, the presence of Ag···O/ O···Ag, C···H/H···C, O···O, Ag···H/H···Ag and O···C/C···O interactions were observed, which are summarized in Table-1.

Conclusion

The IR, UV-visible spectral characteristics and magnetic behaviors of Ag[Cr(1,3-pdta)]·3H$_2$O were described in detail, and Hirshfeld surface analysis was also performed to identify

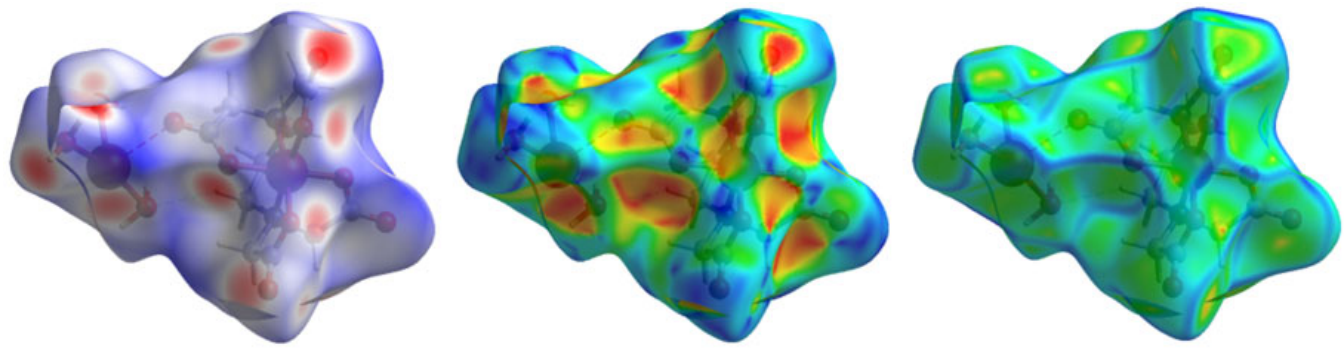

Fig. 7. Hirshfeld surfaces mapped with (a) d_{norm}, (b) shape index and (c) curvedness

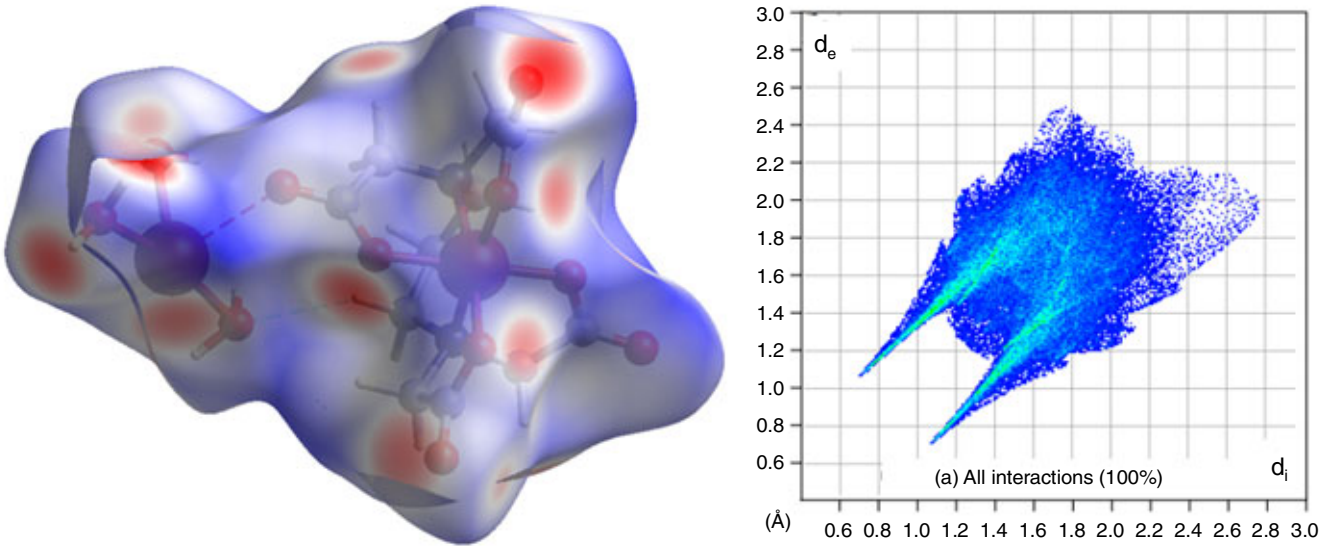

Fig. 8. Hirshfeld surface mapped with (left) d_{norm}, and 2D fingerprint map (right) for all interactions

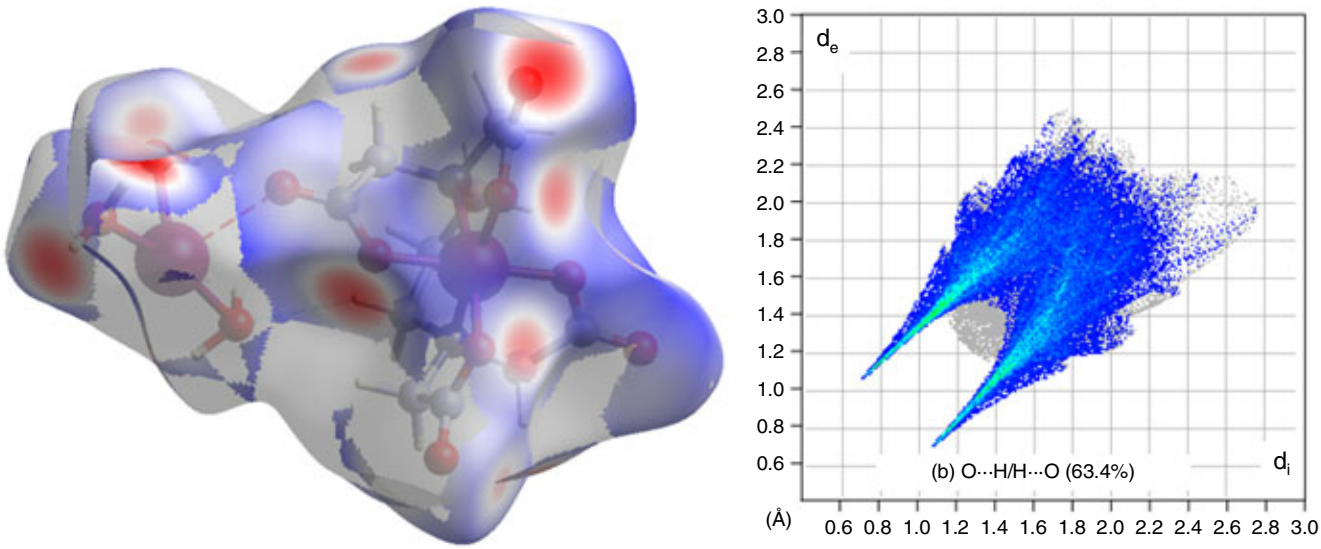

Fig. 9. Hirshfeld surface mapped with (left) d_{norm}, and 2D fingerprint plot (right) for O···H/H···O interactions

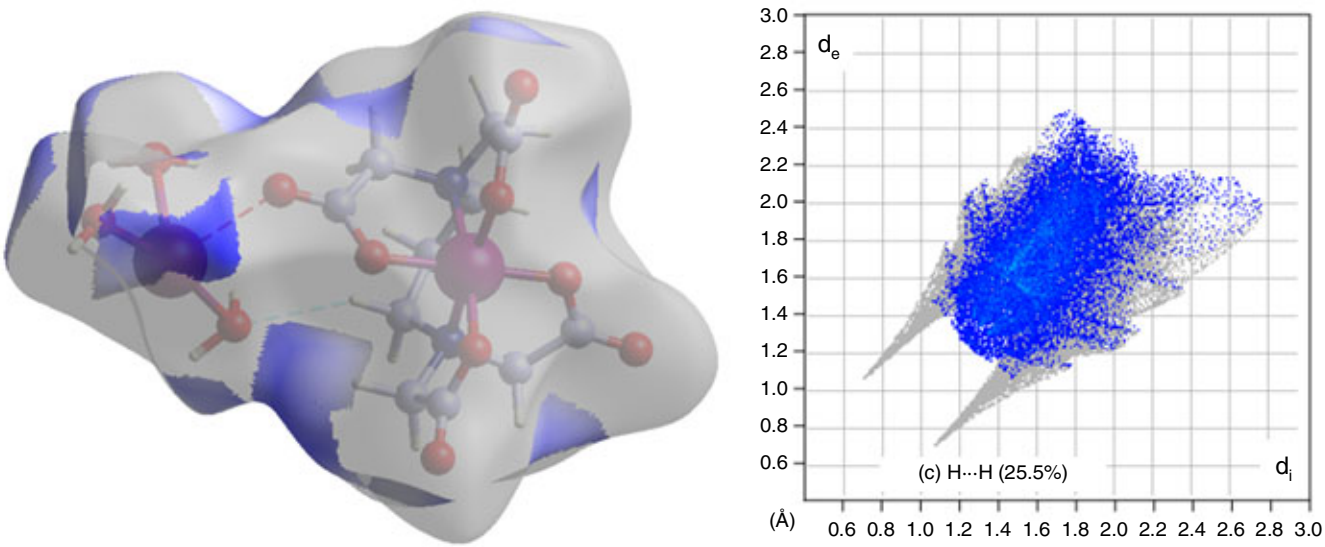

Fig. 10. Hirshfeld surface mapped with (left) d_{norm}, and 2D fingerprint plot (right) for H···H interaction

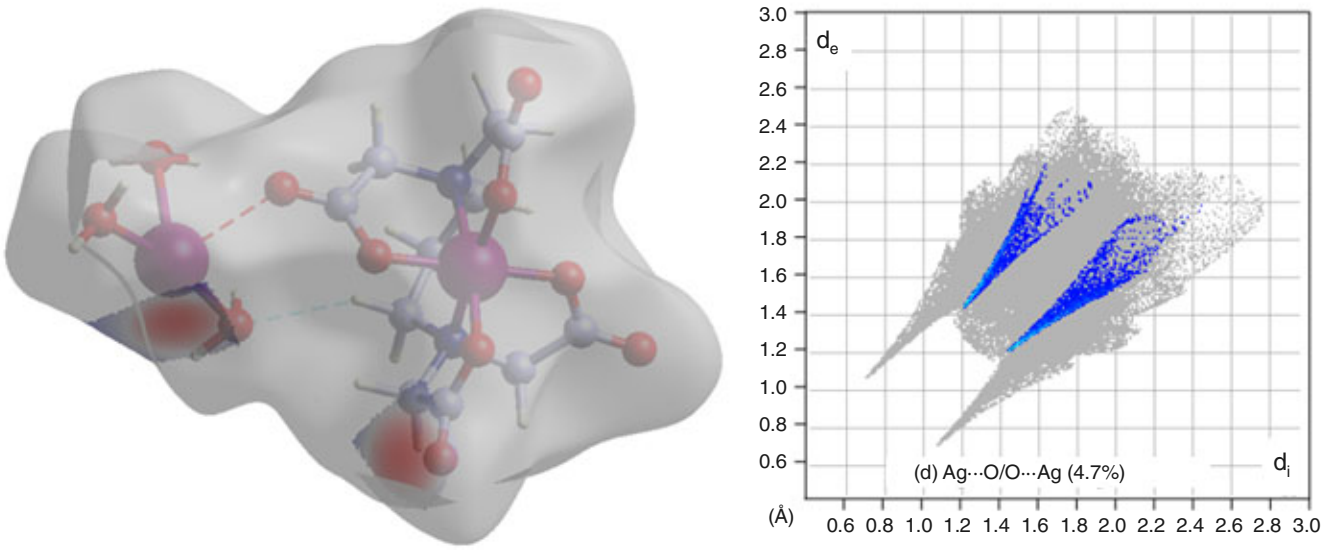

Fig. 11. Hirshfeld surface mapped with (left) d_{norm}, and 2D fingerprint plot (right) for Ag···O/O···Ag interactions

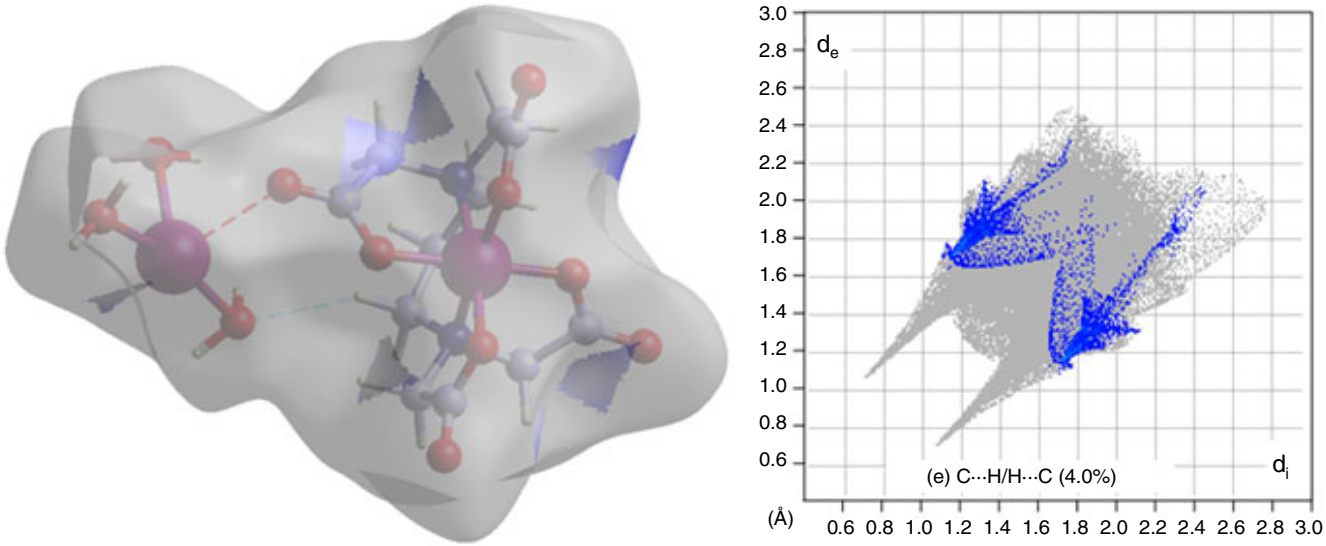

Fig. 12. Hirshfeld surface mapped with (left) d_{norm}, and 2D fingerprint plot (right) for C···H/H···C interactions

TABLE-1
SUMMARY OF VARIOUS CONTACTS AND THEIR CONTRIBUTIONS TO THE HIRSHFELD SURFACE IN Ag[Cr(1,3-pdta)]·3H$_2$O

Types of contacts	Contributions (%)
O···H	63.4
H···H	25.5
Ag···O	4.7
C···H	4.0
O···O	1.4
Ag···H	0.8
O···C	0.2

various intermolecular attraction forces within the crystal. The 1,3-pdta ligand octahedrally coordinate to Cr metal center through four O and two N atoms. The following values were determined for the crystal field splitting and Racah parameters: Dq = 1969 cm^{-1}, B = 594 cm^{-1} and C = 3250 cm^{-1}. Hirshfeld surface analysis with 2D fingerprint plots showed that O···H/H···O (63.4%) and H···H (25.5%) contacts are the main intermolecular interactions. Apart from these above, Ag···O/O···Ag, C···H/H···C, O···O, Ag···H/H···Ag and O···C/C···O contacts have very little contributions of 4.7%, 4.0%, 1.4%, 0.8% and 0.2%, respectively.

ACKNOWLEDGEMENTS

This work was supported by a Research Grant of Andong National University, Andong, Republic of Korea.

CONFLICT OF INTEREST

The authors declare that there is no conflict of interests regarding the publication of this article.

REFERENCES

1. N. Hayashi and T. Akitsu, *Polymers*, **3**, 1029 (2011); https://doi.org/10.3390/polym3031029
2. M.D. Cohen, B. Kargacin, C.B. Klein and M. Costa, *Crit. Rev. Toxicol.*, **23**, 255 (1993); https://doi.org/10.3109/10408449309105012
3. H. Furukawa and T. Akitsu, *J. Chem. Chem. Eng.*, **5**, 207 (2011).
4. S. Kalidhasan, A.S.K. Kumar, V. Rajesh and N. Rajesh, *Coord. Chem. Rev.*, **317**, 157 (2016); https://doi.org/10.1016/j.ccr.2016.03.004
5. R. Nakagame, A. Tsaturyan, T. Haraguchi, Y. Pimonova, T. Lastovina, T. Akitsu and I. Shcherbakov, *Inorg. Chim. Acta*, **486**, 221 (2019); https://doi.org/10.1016/j.ica.2018.10.034
6. Y. Takeshita, K. Takakura and T. Akitsu, *Int. J. Mol. Sci.*, **16**, 3955 (2015); https://doi.org/10.3390/ijms16023955
7. S. Kück, *Appl. Phys. B*, **72**, 515 (2001); https://doi.org/10.1007/s003400100540
8. L.A. Buldt and O.S. Wenger, *Chem. Sci.*, **8**, 7359 (2017); https://doi.org/10.1039/C7SC03372A
9. J.-H. Choi and P.E. Hoggard, *Polyhedron*, **11**, 2399 (1992); https://doi.org/10.1016/S0277-5387(00)83531-7
10. J.-H. Choi, *Chem. Phys.*, **256**, 29 (2000); https://doi.org/10.1016/S0301-0104(00)00097-5
11. J.-H. Choi, *Spectrochim. Acta A Mol. Biomol. Spectrosc.*, **56**, 1653 (2000); https://doi.org/10.1016/S1386-1425(00)00221-3
12. J.-H. Choi, I.G. Oh, T. Suzuki and S. Kaizaki, *J. Mol. Struct.*, **694**, 39 (2004); https://doi.org/10.1016/j.molstruc.2004.01.034
13. J.-H. Choi, Y.P. Hong and Y.C. Park, *Spectrochim. Acta A Mol. Biomol. Spectrosc.*, **58**, 1599 (2002); https://doi.org/10.1016/S1386-1425(01)00611-4
14. J.-H. Choi and S.H. Lee, *J. Mol. Struct.*, **932**, 84 (2009); https://doi.org/10.1016/j.molstruc.2009.05.048
15. J.-H. Choi, *Inorg. Chim. Acta*, **362**, 4231 (2009); https://doi.org/10.1016/j.ica.2009.05.024
16. J.-H. Choi and D. Moon, *J. Mol. Struct.*, **1059**, 325 (2014); https://doi.org/10.1016/j.molstruc.2013.12.008
17. D. Moon and J.-H. Choi, *Spectrochim. Acta A Mol. Biomol. Spectrosc.*, **138**, 774 (2015); https://doi.org/10.1016/j.saa.2014.11.099
18. D. Moon, S. Tanaka, T. Akitsu and J.H. Choi, *Acta Crystallogr. Sect. E*, **71**, 1336 (2015); https://doi.org/10.1107/S2056989015019258
19. N. Górska, E. Mikuli and L. Kótai, *Eur. Chem. Bull.*, **3**, 474 (2014); https://doi.org/10.17628/ecb.2014.3.474-481
20. Y.-S. Dou, *J. Chem. Educ.*, **67**, 134 (1990); https://doi.org/10.1021/ed067p134
21. R.C. Powell, Physics of Solid-State Laser Materials, Springer-Verlag, New York, p. 224 (1998).
22. R. Kripal and A.K. Yadav, *Chem. Phys. Lett.*, **612**, 245 (2014); https://doi.org/10.1016/j.cplett.2014.08.031
23. J.-H. Choi, *Bull. Korean Chem. Soc.*, **11**, 145 (1994).
24. G.M. Cole and B.B. Garret, *Inorg. Chem.*, **9**, 1898 (1970); https://doi.org/10.1021/ic50090a020
25. B.N. Figgis and M.A. Hitchman, Ligand Field Theory and Its Applications; Wiley-VCH: New York (2000).
26. J.R. Gispert, Coordination Chemistry; Wiley-VCH Verlag GmbH & Co KGaA, Weinheim, Germany (2008).
27. M.A. Spackman and D. Jayatilaka, *CrystEngComm*, **11**, 19 (2009); https://doi.org/10.1039/B818330A
28. M.J. Turner, J.J. McKinnon, S.K. Wolff, D.J. Grimwood, P.R. Spackman, D. Jayatilaka and M.A. Spackman, CrystalExplorer17, University of Western Australia (2017).
29. M.A. Spackman and J.J. McKinnon, *CrystEngComm*, **4**, 378 (2002); https://doi.org/10.1039/B203191B
30. D. Moon, S. Tanaka, T. Akitsu and J.-H. Choi, *J. Mol. Struct.*, **1154**, 338 (2018); https://doi.org/10.1016/j.molstruc.2017.10.066
31. T. Aree, Y.P. Hong and J.-H. Choi, *J. Mol. Struct.*, **1163**, 86 (2018); https://doi.org/10.1016/j.molstruc.2018.02.102
32. S. Jeon, J. Moncol, M. Mazúr, M. Valko and J.-H. Choi, *Crystals*, **9**, 336 (2019); https://doi.org/10.3390/cryst9070336
33. J. Moncol, M. Mazúr, M. Valko and J.-H. Choi, *Acta Crystallogr. Sect. C*, **75**, 616 (2019); https://doi.org/10.1107/S2053229619005588